PCCP

Dynamic Article Links

Cite this: *Phys. Chem. Chem. Phys.*, 2012, **14**, 6544–6548

www.rsc.org/pccp

PAPER

From dewetting to wetting molecular layers: C_{60} on $CaCO_3(10\bar{1}4)$ as a case study

Philipp Rahe,* Robert Lindner, Markus Kittelmann, Markus Nimmrich and Angelika Kühnle

Received 17th January 2012, Accepted 8th March 2012
DOI: 10.1039/c2cp40172j

We report the formation of extended molecular layers of C_{60} molecules on a dielectric surface at room temperature. In sharp contrast to previous C_{60} adsorption studies on prototypical ionic crystal surfaces, a wetting layer is obtained when choosing the calcite $(CaCO_3)(10\bar{1}4)$ surface as a substrate. Non-contact atomic force microscopy data reveal an excellent match of the hexagonal lattice of the molecular layer with the unit cell dimension of $CaCO_3(10\bar{1}4)$ in the $[01\bar{1}0]$ direction, while a lattice mismatch along the $[\bar{4}\bar{2}61]$ direction results in a large-scale moiré modulation. Overall, a (2×15) wetting layer is obtained. The distinct difference observed microscopically upon C_{60} adsorption on $CaCO_3(10\bar{1}4)$ compared to other dielectric surfaces is explained by a macroscopic picture based on surface energies. Our example demonstrates that this simple surface-energy based approach can provide a valuable estimate for choosing molecule–insulator systems suitable for molecular self-assembly at room temperature.

1 Introduction

Self-assembly constitutes a powerful strategy for molecular structure formation on surfaces.[1] Consequently, molecular self-assembly has been studied extensively in the past, and a fascinating degree of control has been achieved upon exploiting the subtle balance between intermolecular and molecule–surface interactions of organic molecules on metallic substrates.[2–6] These studies have been further stimulated by the high-resolution capability of scanning tunneling microscopy (STM), allowing for direct imaging of self-assembled structures on metal surfaces at the molecular scale.[7]

On electrically insulating surfaces, however, molecular structure formation has been studied comparatively rarely. This is partly due to experimental challenges associated with the insulating nature of the substrate, hampering the use of a large number of standard surface science techniques including STM. Only recently, non-contact atomic force microscopy (NC-AFM) has been employed for studying fundamental processes in molecular self-assembly on insulating surfaces[8–11] such as C_{60} diffusion on $CaF_2(111)$,[12] formation of hydrogen-bonded networks of benzene diboronic acid molecules on $KCl(001)$[13] or the formation of uni-directional molecular "wires" on $CaCO_3(10\bar{1}4)$.[14]

The self-assembly of organic molecules on insulating surfaces has been mainly hampered by the rather weak molecule–substrate interaction compared to metallic substrates. As a consequence of this weak interaction, dewetting and growth of molecular bulk crystals is typically observed on insulating surfaces at room temperature.[15] Bulk crystal formation, however, is highly undesirable in the context of molecular self-assembly, as tailored structure formation relies on tuning the balance between intermolecular and molecule–substrate interactions. Several strategies have been developed to steer molecular self-assembly on insulating substrates despite the weak molecule–surface interaction, including surface patterning[16,17] and exploiting electrostatic interaction for anchoring polar molecules on ionic crystals.[18,19] So far, however, a simple strategy for the identification of molecule–insulator systems suitable for molecular self-assembly has been largely lacking.

Here, we exploit the concept of macroscopic surface energies for selecting suitable substrates for molecular self-assembly on insulating surfaces. An increased molecule–surface interaction can be achieved when choosing substrates with high surface energies. Comparing various insulating to metallic surfaces, we notice that most insulators studied so far exhibit surface energies considerably smaller by a factor of about ten than typical metal surfaces. An exception is found for the natural cleavage plane of calcite, the $CaCO_3(10\bar{1}4)$ surface, having a surface energy of 590 mJ m^{-2} under ultra-high vacuum (UHV) conditions.[20] We choose the structure formation of C_{60} molecules as an indicator of the wettability and, indeed, we find extended, two-dimensional wetting layers upon deposition of C_{60} onto $CaCO_3(10\bar{1}4)$. This is in sharp contrast to other insulating surfaces such as KBr(100) and NaCl(100), which have substantially smaller surface energies in the order of 100 to 200 mJ m^{-2}. We propose this simple approach, despite relying

Institut für Physikalische Chemie, Fachbereich Chemie, Johannes Gutenberg-Universität Mainz, Jakob-Welder-Weg 11, 55099 Mainz, Germany. E-mail: rahe@uni-mainz.de

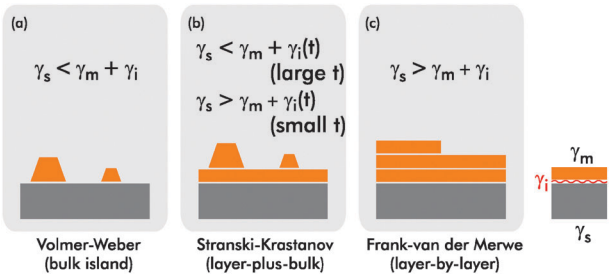

Fig. 1 Growth modes as classified by E. Bauer:[21] (a) Volmer–Weber (bulk island) growth, (b) Stranski–Krastanov (layer-plus-bulk) growth and (c) Frank–van der Merwe (layer-by-layer) growth. The classification is based on macroscopic quantities, namely the surface energies of the substrate (γ_s) and the adsorbate (γ_m) as well as by the interfacial energy γ_i. The quantity t is the film thickness.

on macroscopic quantities, as a first estimate for choosing suitable molecule–surface systems for molecular self-assembly.

Macroscopically, the growth modes can be explained by a simple thermodynamic picture in terms of surface energies.[21] The Volmer–Weber (bulk island) growth mode originates from the fact that the surface energy of the substrate γ_s is smaller than the sum of the surface energies of the molecular bulk crystal γ_m and the interfacial energy γ_i, namely $\gamma_s < \gamma_m + \gamma_i$ (ref. 21). In contrast, for substrate surface energies γ_s larger than the sum of γ_m and γ_i, Frank–van der Merwe (layer-by-layer) growth is favored, resulting in extended, two-dimensional molecular layers:

$$\gamma_s > \gamma_m + \gamma_i. \quad (1)$$

In the intermediate regime, Stranski–Krastanov (layer-plus-bulk) growth is expected as illustrated in Fig. 1. This macroscopic model describes the situation in the thermodynamic equilibrium, which is not necessarily reached if kinetic barriers hinder the growth process. Despite this possibility, however, this approach can provide a valuable estimate for choosing molecule–insulator systems suitable for molecular self-assembly at room temperature. Determining the molecular and in particular the interfacial energy γ_i can be difficult as this energy encompasses system-specific molecule–surface interactions originating from chemical bond formation or chemical polarity of the molecules.[18] However, a high substrate surface energy is always desirable when aiming at extended molecular wetting layers on surfaces rather than bulk crystal formation, as the fulfillment of eqn (1) becomes more likely and allows larger values of the molecular surface energy and the interfacial energy.

A comparison of several surface energies is given in Table 1. As can be seen, the surface energy γ_s of typical metal surfaces is well above 1000 mJ m^{-2}, even for the most close-packed, energetically favorable (111) facets. In sharp contrast, the surface energies of dielectric substrates are typically below 500 mJ m^{-2}, with the frequently studied alkali halide surfaces NaCl(100), KCl(100) and KBr(100) exhibiting very low surface energies in the range of 140 to 180 mJ m^{-2}. Interestingly, the calcite(10$\bar{1}$4) surface presents a significant exception within the class of insulating surfaces having a substantially higher surface energy of 590 mJ m^{-2}. Consequently, according to this simple picture, calcite(10$\bar{1}$4) might constitute a more

Table 1 List of surface energies γ_s reported in the literature. The values reported in the literature differ slightly, the given value is an average

Material	γ_s/mJ m^{-2}	
Metal substrates		
Fe(100)	2714	ref. 27
Pt(111)	2333	ref. 27
Pd(111)	1903	ref. 27
Cu(111)	1877	ref. 27
Au(111)	1332	ref. 27
Ag(110)	1299	ref. 27
Ag(111)	1220	ref. 27
Al(111)	1110	ref. 27
Dielectric substrates		
$CaCO_3$(10$\bar{1}$4)	590	ref. 28–30
CaF_2(111)	480	ref. 31–33
MgO(100)	377	ref. 34
CaO(100)	370	ref. 34
NaF(100)	261	ref. 35–39
NaCl(100)	181	ref. 35–39
KCl(100)	157	ref. 35–38, 40
KBr(100)	141	ref. 35–38
Molecules		
Sexiphenyl(100)	142	ref. 41
C_{60}	116	ref. 24
Pentacene(001)	102	ref. 42
Anthracene(010)	91	ref. 42
Pentacene(010)	47	ref. 42

suitable substrate than the prototypical alkali halide surfaces when aiming at two-dimensional growth of a molecular wetting layer.

Fullerene C_{60} molecules represent a simple and well-studied model system for investigating the principles of molecular growth on insulating surfaces.[9,10,12,22,23] For bulk C_{60}, which condenses in a face-centered cubic (*fcc*) lattice at room temperature, the surface energy γ_m of adjacent close-packed *fcc* planes has been determined to be 116 mJ m^{-2} (ref. 24). Thus, wetting C_{60} layers are expected for C_{60} deposition on metallic surfaces and have been reported for numerous metallic substrates as given in ref. 25 and references therein. In contrast, although the interfacial energy is unknown, it appears reasonable to observe molecular dewetting upon adsorption of C_{60} onto KBr(100), as has, indeed, been obtained.[9,10] In general, only very few examples exist that demonstrate the growth of extended molecular layers on alkali halide (100) surfaces at room temperature, including a hydrogen-bonded network of benzene diboronic acid on KCl(100)[13] and islands of 3,4,9,10-perylene tetracarboxylic dianhydride (PTCDA) on KCl(100)[26] and NaCl(100).[10] Following the simple argumentation based on surface energies made above, the adsorption of C_{60} onto $CaCO_3$(10$\bar{1}$4) might bear the potential of extended wetting layers grown at room temperature. This prediction is validated in the present work.

2 Methods

Optically pure calcite crystals (Korth Kristalle, Altenholz (Kiel), Germany) were cleaved *in situ* using a scalpel.[43] To remove surface charges present after the cleavage step, crystals were annealed to a maximum temperature of ~480 K for 1.5 h. The C_{60} molecules (purity of 99.95% from MER Corporation, Tuscon AZ, USA) were deposited from a home-built Knudsen cell[44,45] onto freshly prepared surfaces held at room temperature. The home-built cell consists of a glass crucible with a tantalum

wire wrapped around. A thermocouple melted into the closed end measures the cell temperature, which is controlled by a current through the Ta wire. The molecular material is inserted into the crucible and protected from dropping out by glass wool. Cell temperatures around 660 K were used, yielding deposition rates in the order of 0.1 ML min^{-1}. Before deposition, the molecules were outgassed for several hours.

NC-AFM experiments were performed at room temperature using an AFM (VT AFM 25 from Omicron, Taunusstein, Germany) operated in the frequency modulation non-contact mode. In this mode, the frequency shift $\Delta f = f - f_0$ of an oscillating cantilever is the main measurement signal.[46] This signal is the difference between the instantaneous resonance frequency f and the resonance frequency f_0 of the freely oscillating cantilever; and it is related to the forces acting between tip and sample.[47] By using a feedback loop, the vertical tip position z is regulated such that the same interaction is sensed by the AFM tip. The selected interaction is given as the frequency shift setpoint Δf_{SP} for all experimental data, together with the scan speed v. For signal demodulation and oscillation excitation, a phase-locked loop detector and amplitude controller (easyPLL plus from Nanosurf, Liestal, Switzerland) was used. As force sensors, Ar-sputtered n-doped silicon cantilevers (type PPP-NCH from NanoWorld, Neuchâtel, Switzerland) with resonance frequencies around 300 kHz were operated at amplitudes of about 10 nm.

3 Results and discussion

Representative, large-scale NC-AFM images obtained after depositing C_{60} molecules onto $CaCO_3(10\bar{1}4)$ are given in Fig. 2. In Fig. 2(a), the equivalent of approximately 1.5 ML was deposited and two step edges of the $CaCO_3(10\bar{1}4)$ substrate are seen, running roughly along the vertical direction in this image as visualized by dotted lines. In the lower part of Fig. 2(a), the height and shape of the C_{60} molecular layers are visualized, the maximum layer height is 4 nm. The edges of the first layer appear smooth. They are significantly different from the edges of the second and third layers, which exhibit a meander shape. This meander shape is well-known for C_{60} growth on C_{60} islands.[48–50] Our NC-AFM data reveal a layer height of about 9.0 ± 1 Å, which is in agreement with previously measured heights of single-layer C_{60} islands on KBr(100) and NaCl(100) surfaces[22] and with the (111)-interplanar distance of 8.7 Å in the C_{60} *fcc* bulk structure.[24] As evident from Fig. 2(a), the steps provide nucleation sites for the C_{60} growth. The overall large-scale morphology does, however, not depend on the presence of step edges as can be seen from Fig. 2(b). In this image, the equivalent of about 0.5 ML C_{60} was deposited and a large number of islands are seen on a terrace plane in the absence of any step edges. The majority of the islands is formed by a single layer with a small second-layer occupation. The edges of the first layer islands appear smooth and resemble those shown in Fig. 2(a). The precise shape may well be influenced by kinetic processes, however, we note the absence of dewetting. This key observation is in sharp contrast to island morphologies observed after deposition of C_{60} on KBr(100), NaCl(100) and $CaF_2(111)$,[22,23] where molecular dewetting has been shown to result in very complex molecular structures.

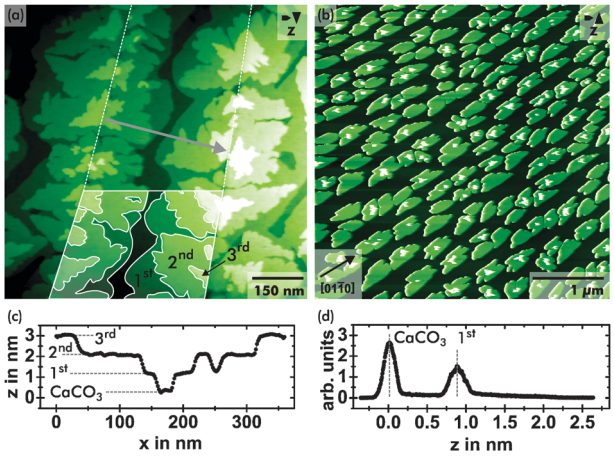

Fig. 2 NC-AFM topography images revealing the C_{60} morphology after deposition onto the $CaCO_3(10\bar{1}4)$ surface. (a) Image with two calcite step edges visualized by dotted lines. In the lower part, the C_{60} layers confined between two step edges are visualized. (b) Similar island structures are observed also in the absence of step edges. (c) Height profile extracted from the indicated line in subfigure (a). The molecular layer heights are indicated. (d) Height distribution from subfigure (b). The substrate and the first layer peak clearly present monomolecular islands (image parameters (a): $\Delta f_{SP} = -5.5$ Hz, $v = 1.74$ μm s^{-1}; (b): $\Delta f_{SP} = -6.8$ Hz, $v = 8.7$ μm s^{-1}).

The molecular layers observed here, in contrast, constitute simple wetting layers with no indication of molecular dewetting such as a second-layer rim or a branched internal structure.

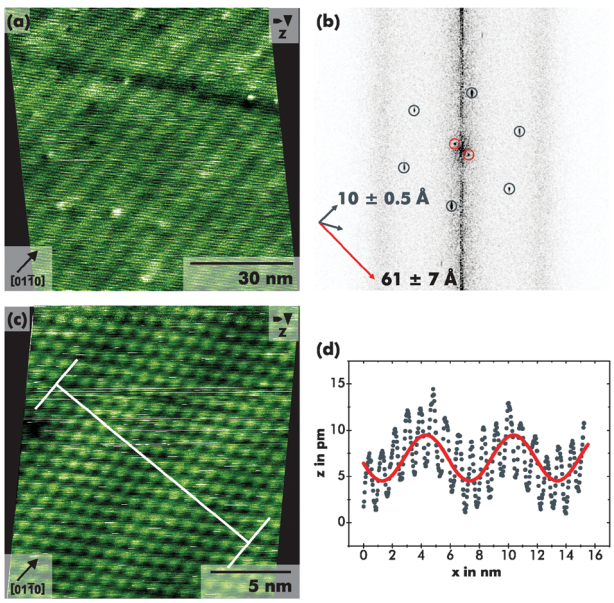

Fig. 3 High-resolution NC-AFM topography images of the $C_{60}/CaCO_3(10\bar{1}4)$ system. (a) Image of the molecular layer revealing a hexagonal pattern and a large-scale moiré pattern. (b) 2D FT data calculated from the image shown in (a) identify a hexagonal structure with a nearest neighbor distance of 10 ± 0.5 Å and a superstructure with a periodicity of 61 ± 7 Å. (c) Zoom into the hexagonal structure. (d) Averaged height profile taken along a line as indicated in (c) revealing both a corrugation of the hexagonal pattern of ~7 pm and of the moiré pattern of ~5 pm (image parameters: (a) $\Delta f_{SP} = -6.2$ Hz, $v = 174$ nm s^{-1}; (c) $\Delta f_{SP} = -13$ Hz, $v = 34.7$ nm s^{-1}. The shown images are corrected for thermal drift.[51]).

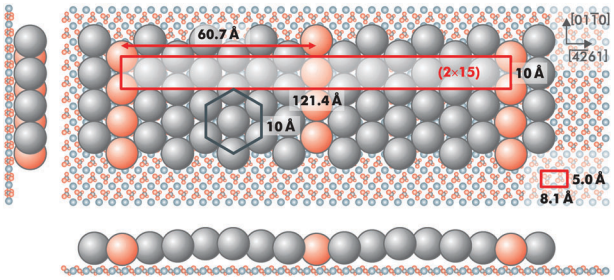

Fig. 4 Proposed model for the C_{60}–$CaCO_3(10\bar{1}4)$ system. The C_{60} molecules form a (2 × 15) superstructure as evident from the NC-AFM experiments. The orientation of the islands with respect to the calcite surface is deduced from our experiments, however, the absolute position is not. Please note that the modulation in the *z* direction is exaggerated for visualization purposes.

To analyze the adsorption configuration in detail, we performed high-resolution NC-AFM imaging on a C_{60} island. Representative data are shown in Fig. 3. We observe a nearly perfect hexagonal structure with a measured nearest-neighbor distance of 10.0 ± 0.5 Å. Additionally, a moiré pattern with a periodicity of 61 ± 7 Å along the [$\bar{4}\bar{2}$61] direction is revealed in our images. These values are obtained from the two-dimensional Fourier transformation (2D FT) data given in Fig. 3(b) and confirmed by carefully drift-corrected[51] NC-AFM images. In Fig. 3(c), the corrugation in the *z*-direction of the C_{60} molecular lattice is measured to be ~7 pm, which is slightly larger than the moiré corrugation of ~5 pm (see Fig. 3(d)).

Based on the measured dimensions, we can propose a model for the C_{60} arrangement on the $CaCO_3(10\bar{1}4)$ surface as depicted in Fig. 4. The hexagonal pattern with a measured lattice constant of 10.0 ± 0.5 Å indicates a hexagonal arrangement of the C_{60} molecules as in the (111) facet of *fcc* C_{60}. The $CaCO_3(10\bar{1}4)$ surface, however, has a rectangular unit cell of 5.0 × 8.1 $Å^2$ in size, as depicted in the lower right corner of Fig. 4. The C_{60} nearest-neighbor distance of 10 Å perfectly matches the twofold substrate periodicity of 5.0 Å in the [01$\bar{1}$0] substrate direction, forming a twofold superstructure. Along the [$\bar{4}\bar{2}$61] direction, however, neither the nearest-neighbor distance of C_{60} nor the plane distance of 8.7 Å formed by close-packed rows fit to the substrate periodicity of 8.1 Å. Consequently, we expect a moiré pattern due to the superposition of the hexagonal C_{60} lattice and the rectangular $CaCO_3(10\bar{1}4)$ lattice. This is, indeed, observed as evident from the large-scale modulation revealed in Fig. 3(c) and (d). The repeat distance of 61 ± 7 Å of the moiré pattern corresponds to 7.5 repeat units of the unit cell dimension in the [$\bar{4}\bar{2}$61] direction, pointing towards a (2 × 15) superstructure. A model of the resulting (2 × 15) structure is depicted in Fig. 4. From our images, we can clearly deduce the orientation of the islands with respect to the underlying calcite lattice as indicated in the NC-AFM data. Furthermore, our model explains the edge shape of the C_{60} islands in Fig. 2(b), where the edges parallel to the [01$\bar{1}$0] substrate direction appear straight compared to the frayed outline for edges oriented along different directions. With our model in Fig. 4, we directly find the energetically more stable edges, where each C_{60} molecule binds to four neighbors, oriented parallel to the [01$\bar{1}$0] direction, while the frayed edges parallel to the [$\bar{4}\bar{2}$61] direction are energetically less stable with only three neighbors for each edge C_{60} atom.

The most important finding of this study is, however, that the observed structures clearly differ from the complex patterns that have been observed on other insulating surfaces as a result of dewetting. A direct comparison is given in Fig. 5. For both KBr(100) and NaCl(100), having very low surface energies of 141 and 181 mJ m^{-2}, a very complex island morphology has been obtained after deposition of C_{60}.[9,22] Also for $C_{60}/CaF_2(111)$ with a surface energy of 480 mJ m^{-2}, a very similar island structure with second-layer rims and a branched internal structure has been observed and clearly related to molecular dewetting.[10,23] Our present data on $CaCO_3(10\bar{1}4)$ reveal that wetting the substrate is energetically more favorable than dewetting. This is in perfect agreement with the surface energy consideration made above, as $CaCO_3(10\bar{1}4)$ has a higher surface energy of 590 mJ m^{-2}.

4 Conclusions

The macroscopic concept of surface energies is adopted to explain the fundamental difference in C_{60} self-assembly on dielectric surfaces. While dewetting has previously been observed for prototypical alkali halide surfaces, a wetting layer is revealed in the present study for C_{60} deposition on $CaCO_3(10\bar{1}4)$, a

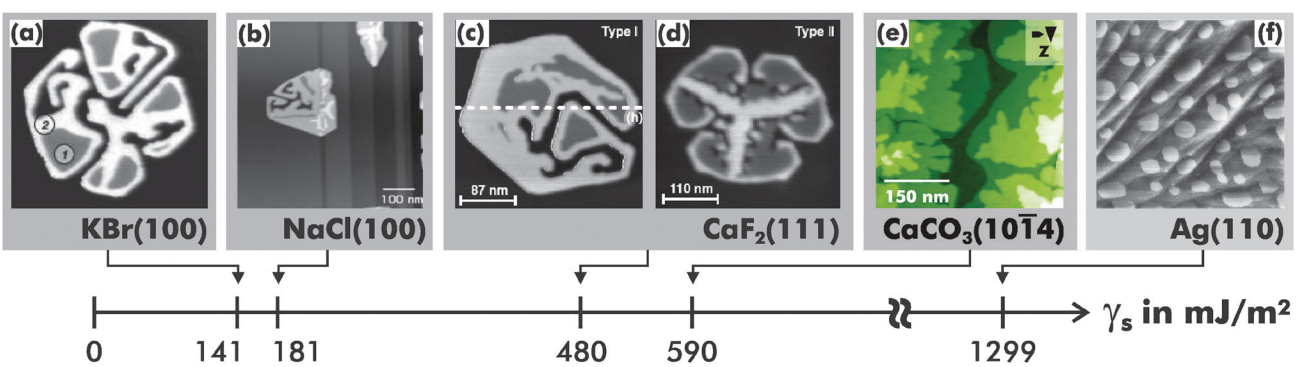

Fig. 5 Comparison of C_{60} adsorption structures on different insulating and metallic surfaces. (a) Dewetted C_{60} island on KBr(100) reproduced with permission from ref. 9. (b) Dewetted C_{60} island on NaCl(100) reproduced with permission from ref. 22. (c) and (d) dewetted C_{60} island on $CaF_2(111)$ reproduced with permission from ref. 23. (e) Wetting islands observed in this study on $CaCO_3(10\bar{1}4)$. (f) Single monolayer islands observed on Ag(111) reproduced with permission from ref. 52 (Subfigures (a), (b), (c), (d) and (f) Copyright 2012 by the American Physical Society).

surface having a substantially higher surface energy than alkali halide surfaces. Our finding is in perfect agreement with the simple consideration of macroscopic surface energies. We suggest that this approach—despite relying on a simple macroscopic thermodynamic concept—can serve as a first estimate to identify molecule–insulator systems suitable for molecular self-assembly at room temperature.

Acknowledgements

Most stimulating discussions with Philipp Maaß and André Gourdon are gratefully acknowledged. This work has been supported by the German Research Foundation (DFG) through the SFB 625 "From Single Molecules to Nanoscopically Structured Materials".

References

1 J. V. Barth, *Annu. Rev. Phys. Chem.*, 2007, **58**, 375.
2 M. Böhringer, W.-D. Schneider and R. Berndt, *Surf. Rev. Lett.*, 2000, **7**, 661–666.
3 G. Pawin, K. L. Wong, K. Y. Kwon and L. Bartels, *Science*, 2006, **313**, 961–962.
4 W. D. Xiao, X. L. Feng, P. Ruffieux, O. Gröning, K. Müllen and R. Fasel, *J. Am. Chem. Soc.*, 2008, **130**, 8910–8912.
5 S. Mohnani and D. Bonifazi, *Coord. Chem. Rev.*, 2010, **254**, 2342–2362.
6 M. Yu, N. Kalashnyk, W. Xu, R. Barattin, Y. Benjalal, E. Lægsgaard, I. Stensgaard, M. Hliwa, X. Bouju, A. Gourdon, C. Joachim, F. Besenbacher and T. R. Linderoth, *ACS Nano*, 2010, **4**, 4097–4109.
7 F. Rosei, M. Schunack, Y. Naitoh, P. Jiang, A. Gourdon, E. Lægsgaard, I. Stensgaard, C. Joachim and F. Besenbacher, *Prog. Surf. Sci.*, 2003, **71**, 95–146.
8 L. Nony, R. Bennewitz, O. Pfeiffer, E. Gnecco, A. Baratoff, E. Meyer, T. Eguchi, A. Gourdon and C. Joachim, *Nanotechnology*, 2004, **15**, S91.
9 S. A. Burke, J. M. Mativetsky, R. Hoffmann and P. Grütter, *Phys. Rev. Lett.*, 2005, **94**, 096102.
10 S. A. Burke, J. M. Topple and P. Grütter, *J. Phys.: Condens. Matter*, 2009, **21**, 423101.
11 O. H. Pakarinen, J. M. Mativetsky, A. Gulans, M. J. Puska, A. S. Foster and P. Grütter, *Phys. Rev. B*, 2009, **80**, 085401.
12 F. Loske, J. Lübbe, J. Schütte, M. Reichling and A. Kühnle, *Phys. Rev. B*, 2010, **82**, 155428.
13 R. Pawlak, L. Nony, F. Bocquet, V. Olson, M. Sassi, J. M. Debierre, C. Loppacher and L. Porte, *J. Phys. Chem. C*, 2010, **114**, 9290–9295.
14 P. Rahe, M. Nimmrich, A. Greuling, J. Schütte, I. Stará, J. Rybáček, G. Huerta-Angeles, I. Starý, M. Rohlfing and A. Kühnle, *J. Phys. Chem. C*, 2010, **114**, 1547–1552.
15 T. Kunstmann, A. Schlarb, M. Fendrich, T. Wagner, R. Möller and R. Hoffmann, *Phys. Rev. B*, 2005, **71**, 121403.
16 L. Nony, E. Gnecco, A. Baratoff, A. Alkauskas, R. Bennewitz, O. Pfeiffer, S. Maier, A. Wetzel, E. Meyer and C. Gerber, *Nano Lett.*, 2004, **4**, 2185–2189.
17 J. M. Mativetsky, S. A. Burke, S. Fostner and P. Grütter, *Small*, 2007, **3**, 818–821.
18 J. Schütte, R. Bechstein, M. Rohlfing, M. Reichling and A. Kühnle, *Phys. Rev. B*, 2009, **80**, 205421.
19 B. Such, T. Trevethan, T. Glatzel, S. Kawai, L. Zimmerli, E. Meyer, A. L. Shluger, C. H. M. Amijs, P. de Mendoza and A. M. Echavarren, *ACS Nano*, 2010, **4**, 3429–3439.
20 N. H. de Leeuw and S. C. Parker, *J. Phys. Chem. B*, 1998, **102**, 2914–2922.
21 E. Bauer, *Z. Kristallogr.*, 1958, **110**, 372.
22 S. A. Burke, J. M. Mativetsky, S. Fostner and P. Grütter, *Phys. Rev. B*, 2007, **76**, 035419.
23 M. Körner, F. Loske, M. Einax, A. Kühnle, M. Reichling and P. Maass, *Phys. Rev. Lett.*, 2011, **107**, 016101.
24 L. A. Girifalco, *J. Phys. Chem.*, 1992, **96**, 858–861.
25 A. J. Maxwell, P. A. Brühwiler, D. Arvanitis, J. Hasselström, M. K.-J. Johansson and N. Mårtensson, *Phys. Rev. B*, 1998, **57**, 7312.
26 T. Dienel, C. Loppacher, S. C. B. Mannsfeld, R. Forker and T. Fritz, *Adv. Mater.*, 2008, **20**, 959.
27 L. Vitos, A. V. Ruban, H. L. Skriver and J. Kollar, *Surf. Sci.*, 1998, **411**, 186.
28 R. Kristensen, S. L. S. Stipp and K. Refson, *J. Chem. Phys.*, 2004, **121**, 8511.
29 D. M. Duffy and J. H. Harding, *J. Mater. Chem.*, 2002, **12**, 3419.
30 N. H. de Leeuw and S. C. Parker, *J. Phys. Chem. B*, 1998, **102**, 2914.
31 J. J. Gilman, *J. Appl. Phys.*, 1960, **31**, 2208.
32 N. H. de Leeuw and T. G. Cooper, *J. Mater. Chem.*, 2003, **13**, 93.
33 V. E. Puchin, A. V. Puchina, M. Huisinga and M. Reichling, *J. Phys.: Condens. Matter*, 2001, **13**, 2081.
34 W. Liu, X. Liu, W. T. Zheng and Q. Jiang, *Surf. Sci.*, 2006, **600**, 257.
35 F. Van Zeggeren and G. C. Benson, *J. Chem. Phys.*, 1957, **26**, 1077.
36 P. W. Tasker, *Philos. Mag. A*, 1979, **39**, 119.
37 G. C. Benson and T. A. Claxton, *J. Chem. Phys.*, 1968, **48**, 1356.
38 R. Shuttleworth, *Proc. Phys. Soc., London, Sect. A*, 1949, **62**, 167.
39 W. C. Mackrodt and R. F. Stewart, *J. Phys. C: Solid State Phys.*, 1977, **10**, 1431.
40 D. M. Heyes, M. Barber and J. H. R. Clarke, *J. Chem. Soc., Faraday Trans.*, 1977, **73**, 1485.
41 D. Nabok, P. Puschnig and C. Ambrosch-Draxl, *Phys. Rev. B*, 2008, **77**, 245316.
42 J. E. Northrup, M. L. Tiago and S. G. Louie, *Phys. Rev. B*, 2002, **66**, 121404.
43 L. Tröger, J. Schütte, F. Ostendorf, A. Kühnle and M. Reichling, *Rev. Sci. Instrum.*, 2009, **80**, 063703.
44 M. Knudsen, *Ann. Phys. (Berlin, Ger.)*, 1909, **28**, 999–1016.
45 P. Clausing, *Z. Phys. A: Hadrons Nucl.*, 1930, **66**, 471–476.
46 T. R. Albrecht, P. Grütter, D. Horne and D. Rugar, *J. Appl. Phys.*, 1991, **69**, 668–673.
47 F. J. Giessibl and H. Bielefeldt, *Phys. Rev. B*, 2000, **61**, 9968–9971.
48 R. Lüthi, E. Meyer, H. Haefke, L. Howald, W. Gutmannsbauer and H. J. Güntherodt, *Science*, 1994, **266**, 1979–1981.
49 H. Liu, Z. Lin, L. V. Zhigilei and P. Reinke, *J. Phys. Chem. C*, 2008, **112**, 4687–4695.
50 H. Liu and P. Reinke, *J. Chem. Phys.*, 2006, **124**, 164707.
51 P. Rahe, R. Bechstein and A. Kühnle, *J. Vac. Sci. Technol., B*, 2010, **28**, C4E31.
52 T. David, J. K. Gimzewski, D. Purdie, B. Reihl and R. R. Schlittler, *Phys. Rev. B*, 1994, **50**, 5810–5813.

